Analysis of Sub-τc and Supra-τc Motions in Protein Gβ1 Using Molecular Dynamics Simulations

4 AUTHORS, INCLUDING:

Michele Vendruscolo
University of Cambridge

346 PUBLICATIONS **12,360** CITATIONS

SEE PROFILE

Analysis of Sub-τ_c and Supra-τ_c Motions in Protein Gβ1 Using Molecular Dynamics Simulations

Jennifer M. Bui,[†][*] Jörg Gsponer,[‡] Michele Vendruscolo,[†] and Christopher M. Dobson[†]
[†]Department of Chemistry, University of Cambridge, Cambridge, United Kingdom; and [‡]MRC Laboratory of Molecular Biology, Cambridge, United Kingdom

ABSTRACT   The functions of proteins depend on the dynamical behavior of their native states on a wide range of timescales. To investigate these dynamics in the case of the small protein Gβ1, we analyzed molecular dynamics simulations with the model-free approach of nuclear magnetic relaxation. We found amplitudes of fast timescale motions (sub-τ_c, where τ_c is the rotational correlation time) consistent with S^2 obtained from spin relaxation measurements as well as amplitudes of slow timescale motions (supra-τ_c) in quantitative agreement with S^2 order parameters derived from residual dipolar coupling measurements. The slow timescale motions are associated with the large variations of the ^3J couplings that follow transitions between different conformational substates. These results provide further characterization of the large structural fluctuations in the native states of proteins that occur on timescales longer than the rotational correlation time.

INTRODUCTION

Nuclear magnetic resonance (NMR) spectroscopy offers powerful tools to investigate structures and dynamics of proteins in solution over a large range of timescales (1–4). NMR relaxation measurements provide information about dynamics on the picosecond to nanosecond timescale (1,4,5). In addition, the detection of motions up to the millisecond range, derived from measurements of residual dipolar couplings (RDCs) in different alignment media, provides key information about slower, biologically relevant motions in proteins (6–9). As a complement to these experimental studies, molecular dynamics (MD) simulations have become an increasingly effective tool to investigate protein motions (10–14) particularly for motions taking place on timescales longer than the rotational correlation time τ_c, the so-called supra-τ_c motions (9).

In this study, we investigate the multiple timescale motions of the small protein Gβ1 by carrying out submicro-second MD simulations at two different protonation states: i), to mimic pH conditions (4.0) under which NMR relaxation measurements were previously conducted (15,16); and ii), at neutral pH (7.0). Using the model-free approach (5) to analyze the dynamics of this small protein, we find that the amplitudes of the fast timescale motions are in agreement with S^2 order parameters obtained from spin relaxation measurements (15) whereas the amplitudes of the slow motions are consistent with RDC measurements (17,18). In particular, we find large variations of ^3J couplings for residues that exhibit slow timescale motions. Such variations of ^3J couplings are caused by transitions between different conformational substates. These transitions, which leave clear signatures in the autocorrelation functions, are

observed mainly in residues that change conformation in different functional states of Gβ1.

METHODS

MD simulations

The immunoglobulin-binding domain β1 of the streptococcal protein G (Gβ1) is a small 56-residue single domain protein comprising an α helix and a four-stranded β-sheet (19). First, pronotation states for all titratable residues of the NMR 1GB1 ensemble (19) were determined. The effective pKa for each titratable group was computed using the WHATIF pKa calculation package as described previously (20). The linearized Poisson-Boltzmann equation was computed using a dielectric constant of four for the protein and by the Delphi Poisson-Boltzmann electrostatic solver (21). The average pKa value of each titratable group is reported in Table S1 in the Supporting Material. Because NMR relaxation experiments and RDC measurements have previously been carried out under different pH conditions, two MD simulations were carried out: i), MD-pH4 in which E15, E19, D22, D36, D40, D46, and D47 were protonated to mimic pH 4.0 conditions (Table S1); and ii), MD-pH7, where the same residues were deprotonated (15,17,22). Three chloride ions were then added to neutralize the MD-pH4 system. In contrast, four sodium ions were added to the MD-pH7 system. Both systems were solvated with 3281 and 3215 TIP3P water molecules for MD-pH4 and MD-pH7 systems, respectively (23).

MD simulations were carried out using the modified AMBER ff99SB force field (24,25). Initial 1000 steps of steepest descent energy minimization were followed by the reassignments of velocities from the Maxwell distribution at 300 K every 1 ps for 100 ps, and by a final equilibration of the system for 1000 ps. After equilibration, the MD trajectories were integrated using the PMEMD module of AMBER 9 (26). The simulations were conducted using the isobaric-isothermal ensemble (27) at 300 K and 1 atmosphere and using long-range nonbonded interactions with a 12 Å residue-based cutoff. Long-range electrostatic forces were calculated using the particle-mesh Ewald sum (28). Bonds to hydrogen atoms were maintained with the SHAKE algorithm (29) and an integration step size of 2 fs was used. The simulations were carried out for 177 ns and 87 ns for MD-pH4 and MD-pH7, respectively. The root mean-square deviation of the backbone atoms were monitored and within 2.5 Å of their reference frames (i.e., the first snapshots after equilibrations) for MD-pH4 and MD-pH7 (Fig. S1). To further ensure sufficient equilibrations of the system, we

---

discarded the first 2 ns and analyzed results of the last 175 ns and 85 ns of the MD-pH4 and MD-pH7, respectively.

Autocorrelation functions and the model-free approach

According to spin relaxation theory (30), the spectral density function is the Fourier transform of the angular autocorrelation function, $C(t)$, of the N-H bond vector

$$J(\omega) = 2 \int_0^\infty C(t)\cos(\omega t)dt. \qquad (1)$$

Assuming that the overall molecular tumbling is slower than the internal motions, $C(t)$ can be decomposed into the product of the correlation functions for the overall tumbling, $C_O(t)$ and for the internal motion, $C_I(t)$. The internal motion correlation function can be expressed as (5)

$$C_I(t) = \left\langle P_2\big(\widehat{\mu}(0) \times \widehat{\mu}(t)\big)\right\rangle, \qquad (2)$$

where the second Legendre polynomial $P_2(x) = (3x^2 - 1)/2$, and the unit vector $\widehat{\mu}$ describes the orientation of the N-H bond vector. To compare internal motions that occur on timescales shorter and longer than the rotational correlation time of 3.3 ns (obtained from the analysis of T1/T2 ratios of the ^1H-^{15}N NMR measurements (15)), the MD trajectories were divided into small intervals of 10 ns length. N-H vector autocorrelation functions, $C_I(t)$, were calculated for these intervals or the entire trajectory after each frame of the MD trajectory was superimposed to the first frame using quaternion fitting. The correlation functions were then fitted using either the original model-free approach (5)

$$C_I(t) = S^2 + \big(1 - S^2\big)e^{-t/\tau e}, \qquad (3)$$

or its extended version with four motional parameters (31)

$$C_I(t) = S^2 + \big(1 - S_f^2\big)e^{-t/\tau_f} + \big(S_f^2 - S^2\big)e^{-t/\tau_s}, \qquad (4)$$

where S^2 is the generalized order parameter; S_f^2 is the order parameter for fast motions; and τ_f and τ_s are the correlation times for the fast and slow motions, respectively. For the 10-ns intervals, an average S^2 parameter was calculated by averaging of the 17 S^2 values that resulted from the fitting of the 17 trajectory segments.

RESULTS

Sub-τ_c and supra-τ_c motions in Gβ1

To investigate the different timescale motions in Gβ1 and compare them with NMR data, a 175 ns MD trajectory was obtained for the protonation state mimicking pH 4.0 conditions (see Methods). N-H bond autocorrelation functions (Eq. 2) were then calculated both for the entire simulation and for short intervals of 10 ns length. The autocorrelation functions of all backbone N-H bonds were then fitted using the first (Eq. 3) or second (Eq. 4) model-free approach (Methods). The average S^2 values of 17 10-ns MD trajectory segments are reported in Table S2. Consistent with previous studies (32,33), two main classes of correlation functions were observed: i), those with a rapid decay to a stable plateau (class 1); and ii), those with a slow convergence to a stable plateau (class 2, Fig. 1). For the correlation
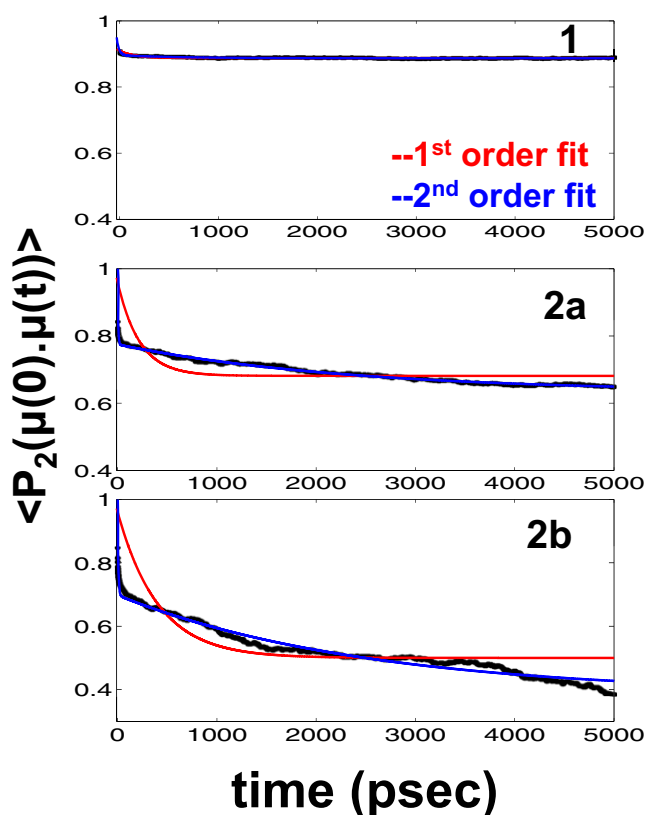

FIGURE 1 Classification of autocorrelation functions, $C_I(t)$. A rapid decay due to libration motions, from $C_I(0) = 1$ to a value typically near 0.90–0.93, is followed by: (1) a rapid convergence to a stable plateau; (2a) a smooth decay to a stable plateau; and (2b) a converging decay with reflections that are the result of transitions between different conformational substates.

functions of class 1, no significant differences were found between the S^2 order parameters obtained using the first or second order fitting, Eq. 3 and Eq. 4, respectively (Tables S2 and S3). In contrast, those of the class 2 are better fitted with Eq. 4 and converge to lower plateaus in the full-length trajectory than in the 10-ns segments (Tables S2 and S3). Consistently, the fitting is significantly improved when using Eq. 4 instead of Eq. 3 (i.e., the magnitude of the change of the R^2 value is more pronounced for class 2 than class 1; Tables S2 and S3). For instance, the fittings of the correlation functions of residues 18–35, which belong to class 1, with either Eq. 3 or Eq. 4 do not result in any sizable difference between the S^2 parameters and only a minor change in the magnitude of the R^2 values. Hence, using the second model-free approach for these residues is not necessary. However, for residues with correlation functions of the class 2 (e.g., residues 9–14), the S^2 order parameters obtained from Eq. 4 are significantly different from those obtained from Eq. 3, and considerable improvements of the R^2 values result from the use of Eq. 4. For these residues, the second order model-free approach provides estimates of relaxations rates for slow and fast motions that have differences of up to three orders of magnitude (Tables S2 and S3).

Comparison of the S^2 parameters resulting from these calculations with those derived from NMR measurements shows that order parameters of the sub-τ_c ($t < \tau_c$) intervals are highly correlated with those obtained from NMR spin-relaxation experiments (Fig. 2 A). By contrast, although S_f^2 parameters are similar to the order parameters derived from NMR spin-relaxation experiments when the full-length trajectory is fitted, S^2 parameters are highly correlated with S_{RDC}^2 parameters derived from RDC measurements (17,18) (Fig. 2, B and C). Consistent with the RDC measurements and previous RDC-restrained MD simulations (9,17,18), we find motions in the supra-τ_c ($\tau_c < \tau_s < \mu$s) regime predominantly in regions where residues adopt different conformational substates. More specifically, slow motions are observed for residues in the highly flexible region of β-strand 2, which mediates interactions between protein Gβ1 and its antigen-binding partner IgG (17), and the turn connecting the α-helix and the β-strand 3. This turn has been observed to adopt a conformation in a domain-swapped dimer that is different from the wild-type one (see below) (34). The second class of correlation functions can be further divided into two types: those for which $C(t)$ displays a smooth decay (2a), and those for which $C(t)$ exhibits small ''bumps'' that are the result of transitions between conforma-
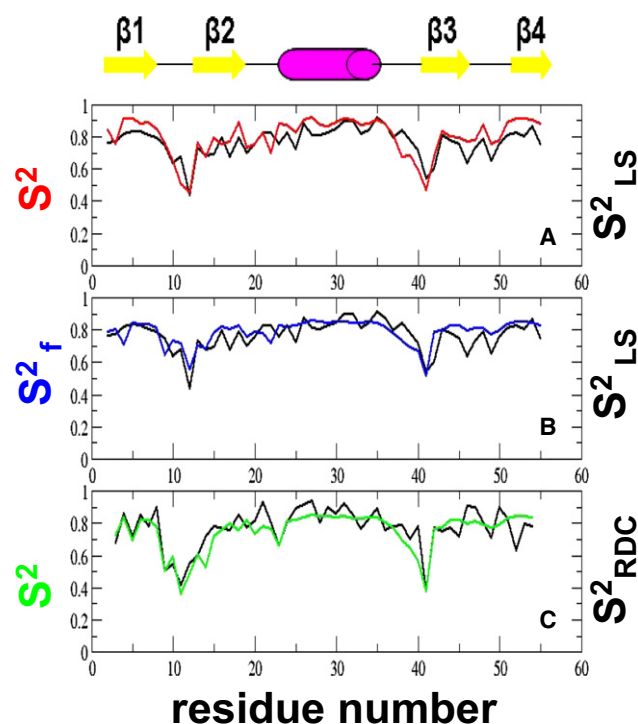
tional substates (2b) (35) (Fig. 1). This classification is consistent with the one used by Showalter and Bruschweiler (33). However, here the correlation functions in class 2b converge in most cases to stable plateaus because multiple transitions between substates are observed during the course of the simulation (Figs. 3 and 4).

Conformational transitions in the supra-τ_c regime

To explore these conformational transitions, backbone dihedral angles were calculated for several residues that display motions in the supra-τ_c regime, i.e., residues at the tip of the linker loops between the β-strands 1 and 2, and the α-helix and the β-strand 3. We found that residue T11, for example, populates two conformational substates, one with $\Phi \approx -80°$ and another with $\Phi \approx -130°$ (Fig. 3). Transitions between these substates are reflected on the autocorrelation function (class 2b). To analyze motions within the two substates, the full-length MD trajectory was divided into segments with relatively constant torsion angles and correlation functions calculated for each segment individually. The correlation functions show a fast decay when calculated for segments where T11 populates the substate with $\Phi \approx -80°$ and a slow decay for segments where $\Phi \approx -130°$. Structural examination of the latter substate showed that restricted backbone motions cause the slow decay, i.e., the methyl group of T11 stacks against a hydrophobic pocket formed by L12, V39, and N37. By contrast, the fast decay of the correlation function is possible when
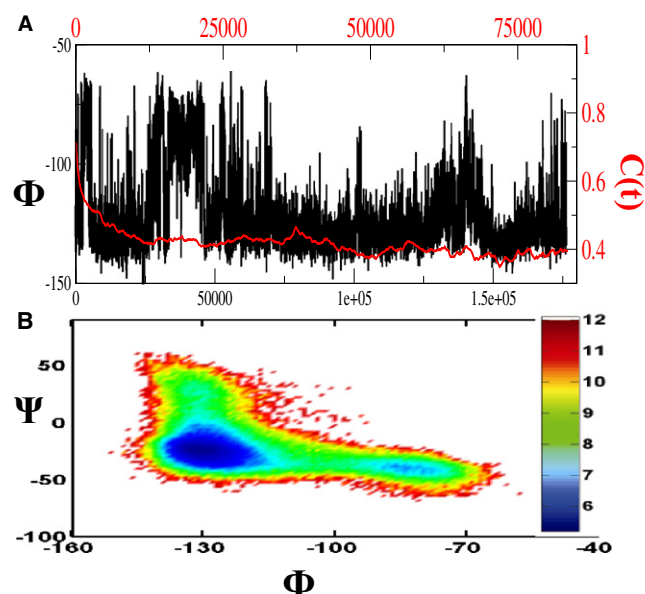
FIGURE 2 Comparisons between computed (*colored lines*) and experimental (*black lines*) S^2 order parameters. (A) S^2 values (*red*) are obtained by fitting the autocorrelation functions of the 10-ns intervals (Table S2); (B) S_f^2 (*blue*); and (C) S^2 (*green*) values are obtained by applying the second order model-free approach to the autocorrelation function calculated for the 175 ns MD trajectory (Table S3). The secondary structures are depicted as yellow arrows for β-strands and purple for the α-helix.

FIGURE 3 Dynamic transitions of residue T11. (A) Torsion angle ϕ of T11 as function of time (*black line* scaled on the left axis), and its correlation function (*red line* scaled on the right axis). Small ''bumps'' on the correlation function reflect transitions between two conformational populations centered at $\phi = -130°$ and $\phi = -80°$. (B) Probability distribution for the sampling of the two conformers. The color bar has a unit of RT, where R is the gas constant and T is a temperature.
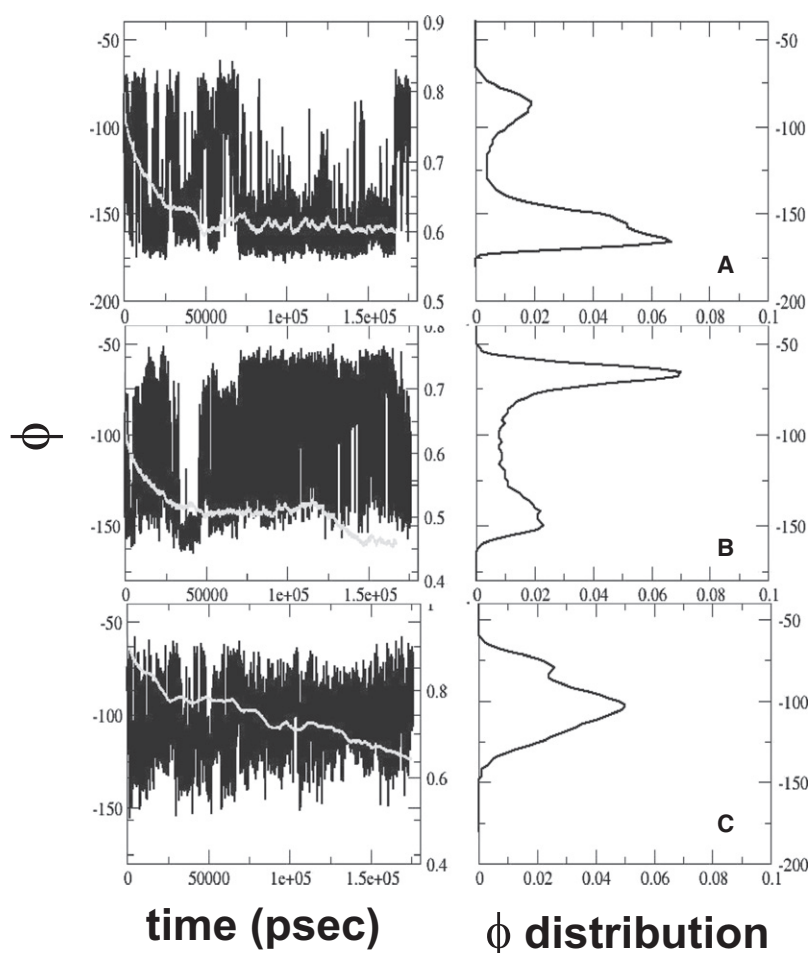
FIGURE 4 Analysis of the impact of conformational transitions onto the autocorrelation functions for residues (A) K10; (B) L12; and (C) D40. The dihedral angles Φ and the $C_I(t)$ of these residues are plotted as functions of time (*left column*). (*Right column*) Distributions of different Φ populations.

the methyl group of the T11 side chain is solvent-exposed. Similar transitions between substates were observed for residues K10, L12, and D40 (Fig. 4) during the 175 ns MD simulation. The relaxation times within theses substates can vary significantly and (in some cases) take much longer time than the rotational correlation time τ_c as can be seen in Fig. 3, where T11 is in the region of $\Phi \approx -80°$ for >25 ns (35).

The transitions between different conformational substates for functionally important residues should be reflected in the distribution of the $^3J_{HNH\alpha}$ coupling constants (36). $^3J_{HNH\alpha}$ coupling constants for each residue were, therefore, computed using various reparameterized Karplus coefficients (37–40). The best agreement between the averages of computed $^3J_{HNH\alpha}$ couplings and the experimental $^3J_{HNH\alpha}$ couplings measured by Clore (41) is found when Karplus coefficients from Hu and Bax (39) were used (a correlation coefficient of 0.945, Fig. 5). Similarly good results were obtained when using Karplus coefficients that had recently been derived from a fit of high-confidence J-coupling measurements (a correlation coefficient of 0.926 between Vogeli et al. (37) $^3J_{HNH\alpha}$ couplings and those of the MD-pH4 ensemble, data not shown). It is of importance to note that the recent multiple-quantum J-splitting measurements by Vogeli et al. (37) identify the highly mobile residues in

the supra-τ_c time range in the same protein regions that we and others did (17). Distributions of the $^3J_{HNH\alpha}$ couplings are different for residues with or without motions in the supra-τ_c range—i.e., we find a bimodal distribution for the former and a narrow distribution for the latter (Fig. 6, A and B, and Fig. S2). Significantly larger variances in $^3J_{HNH\alpha}$ couplings are found for residues that exhibit slow motions such as K10, T11, L12, V39, D40, and G41 ($p = 0.0021$). Fig. 6 and Fig. S2 also show that the average ^3J couplings obtained from the MD simulations are close to the experimental measured values (averaged over all conformations) but that the widths of the distributions are rather large. More specifically, Fig. 6 A shows that ~8.0% of the sampled conformers of residue V39 have $^3J_{HNH\alpha}$ couplings (6.20) that are much smaller than the measured average value of 9.86. In these conformers, the linker loop residue V39 coils up and adopts a tertiary structure as observed in the domain-swapped dimer (Fig. 6 D) (34).

Convergence and pH dependence of motions in the supra-τ_c regime

We found that order parameters derived from the fitting of correlation functions of residues with motions in the
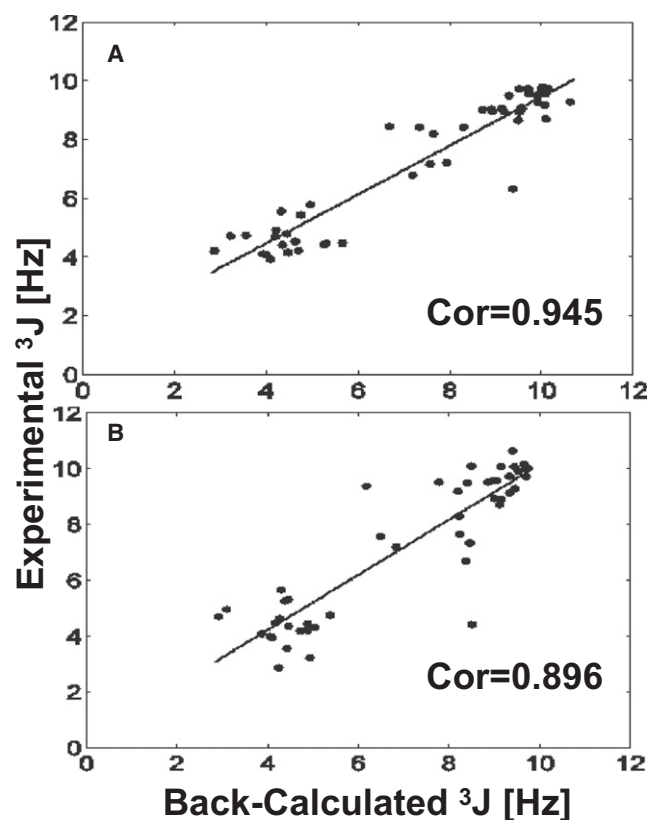
FIGURE 5 Correlation between experimental and computed $^3J_{HNH\alpha}$ coupling constants for (A) MD-pH4 and (B) MD-pH7.

supra-τ_c range are in very good agreement with S^2 parameters derived from RDC measurements despite the fact that the timescale of the MD trajectory is much shorter than the one probed experimentally. This result seems to indicate that the motions of most these residues are, if not fully then at least partially, converged in the timescale of the

simulation. To test the extent of convergence, we divided the simulation in half, refitted the correlation functions of this 85 ns long trajectory, and compared the S^2 order parameter results. We found no significant difference in correlation coefficients between the computed and experimentally calculated S^2 order parameters for the 85 ns and 175 ns MD-pH4 trajectories (0.73 and 0.77, respectively; Fig. 7). However, the correlation between experimental and calculated S^2 order parameters is slightly better for the full-length 175 ns trajectory when only residues with motions in the supra-τ_c range (Fig. 7), i.e., residues on the tip of the linker loop between the β-strands 1 and 2 as well as the linker between the α-helix and β-strand 3, are compared.

The 175 ns MD trajectory (MD-pH4) was carried out for the protonation state that mimics the experimental conditions under which the structure of Gβ1 was determined and NMR relaxation data collected initially (15,19,42). In the light of the good agreement between the calculated S^2 order parameters of residues with motions in the supra-τ_c range and RDC data, it is important to note that RDC data had been collected at a slightly higher pH of 6.5 (22). To investigate whether this agreement is a result of the protonation state setup, an 85-ns MD simulation (MD-pH7) was carried out for a canonical protonation state that mimics pH 7 conditions (see Methods). Using the same fitting procedure as for the MD-pH4, we determined S^2 order parameters for the MD-pH7 and compared them to the RDC-derived order parameters. Interestingly, order parameters calculated from the correlation functions of the MD-pH4 show a significantly better correlation with the RDC-based S^2 order parameters than those order parameters calculated from MD-pH7 (0.73 vs. 0.55; Fig. S3). We also compared the computed $^3J_{HNH\alpha}$ coupling constants of the MD-pH7 and MD-pH4 trajectories. As can be seen in Fig. 5, the MD-pH4 has a slightly higher correlation coefficient than the MD-pH7.
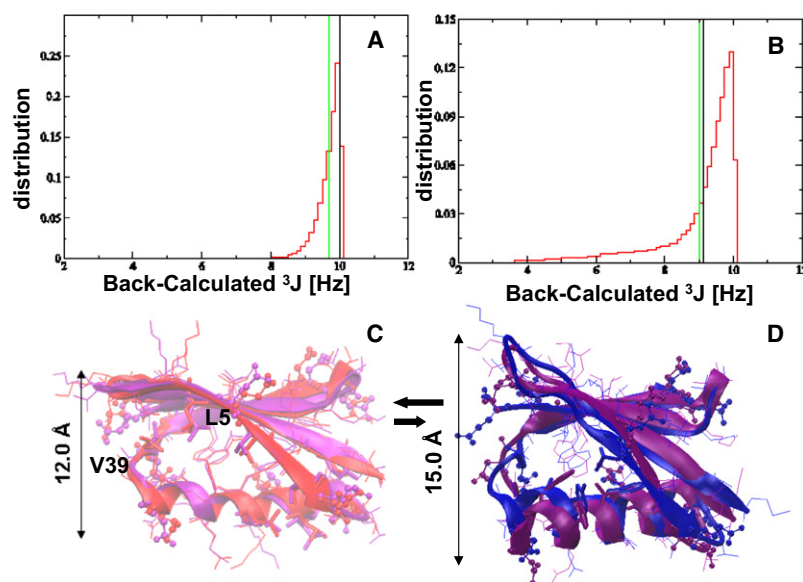

FIGURE 6 Comparison of $^3J_{HNH\alpha}$ coupling constants for residues with or without motions in the supra-τ_c range. (A) The distribution of the $^3J_{HNH\alpha}$ coupling constants of L5 (red line) computed for all snapshots of the full-length MD trajectory. The green line indicates the average value computed over all sampled conformations. The black line indicates the experimental measured value. (B) The distribution of the $^3J_{HNH\alpha}$ coupling constants of V39 (red line) computed for all snapshots of the full-length MD trajectory. The green line indicates the average value computed over all sampled conformations. The black line indicates the experimental measured value. (C) An average structure (red) calculated from those snapshots in which $^3J_{HNH\alpha}$ coupling constants of V39 $\approx$ 9.8 is compared to the initial structure (purple). (D) An average structure (blue) calculated from those snapshots in which $^3J_{HNH\alpha}$ coupling constants of V39 $\approx$ 6.2 is compared to the domain-swapped dimer structure (purple, PDB:1Q10).
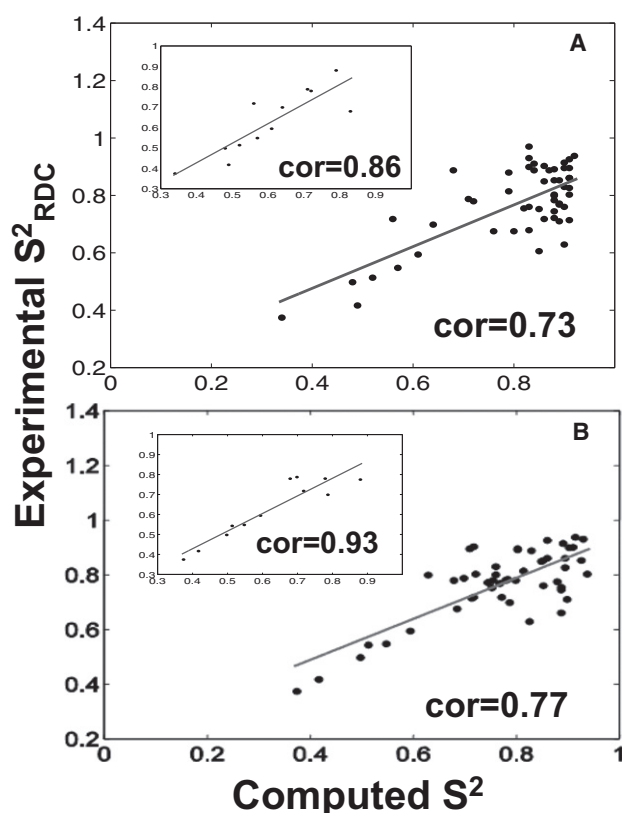
FIGURE 7 Correlation between the S^2_{RDC} values and the 2nd order fitting S^2 values computed from the (A) 85 ns MD-pH4 segment and the (B) 175 ns MD-pH4 trajectory. The insets show the correlation coefficient computed for residues that exhibit the supra-τ_c motions.

DISCUSSION

Conformational fluctuations of proteins in their native states play an important role for their function. Advances in NMR spectroscopy have allowed localizing and defining the magnitude of protein motions over a wide range of timescales. Concomitantly, improved force fields and increasing computer power have enhanced our ability to characterize the atomistic details of protein dynamics by MD simulations (10,12–14). Particularly for motions occurring in the picosecond to nanosecond timescale, qualitative agreement between relaxation rates and order parameters obtained from MD simulations and those derived from experiments has been observed (13,32). In addition, significant insight into the characteristics of the motions on longer timescales has been obtained (10,13,14). However, it has been proposed that MD simulations can overestimate backbone flexibility in loop regions of proteins in the sub-τ_c timescale (faster than the overall rotational diffusion) due to a relative imbalance between the description of hydrogen bonding and other force field terms (12). In this sense, it is particularly interesting that motions probed by relaxation experiments, which are limited to a time range up to the overall rotational diffusion, are averaged over ensembles of conformational substates sampled

in the supra-τ_c timescale. The sampling of these ensembles of conformational substates by classical MD simulations remains a significant challenge.

In this work, we have carried out submicrosecond MD simulations of Gβ1 in different protonation states and fitted the correlation functions of backbone N-H bond vectors using the model-free formalism with either two or four free parameters. Our results show clearly that, for this protein, the amplitudes of the backbone motions in the sub-τ_c timescale are not overestimated when compared to experimentally derived S^2_{LS} parameters (Tables S2 and S3). However, some residues display also slow motions occurring in the supra-τ_c timescale, which is reflected in better fits of the correlation function of the full length MD trajectory by the extended model-free formalism and τ_s in the upper nanosecond time range (Table S3). Interestingly, these motions accurately reproduce the amplitudes of the slow motional modes derived from RDC measurements in different alignment media (17,18). Similar to our findings, Showalter and Bruschweiler reported recently that an ensemble of ubiquitin extracted from a 50-ns MD simulation shows remarkable agreement with S^2_{RDC} (13). Because RDC measurements probe motions that can take place up to the millisecond timescale, to reproduce them, it is, therefore, expected that much longer MD simulations up to millisecond timescale should be carried out. However, our finding that, for the protein that we considered, order parameters derived from the 175-ns MD trajectory are in excellent agreement with those derived from multiple RDC measurements seems to indicate that the conformational sampling of residues with motions in the supra-τ_c range is already partially converged (Fig. 7). One possibility is that this protein does not exhibit additional dynamics up to the millisecond timescale other than those that we sampled on the much shorter timescale of our simulations. Interestingly, a better quantitative agreement both with J-couplings and with S^2_{RDC} (Figs. 5 and 7) is observed for the simulation mimicking pH 4.0 conditions. This result is intriguing because RDC measurement had been carried out above pH 4.0. Perhaps, it could be attributed to the simulation conditions that facilitate the sampling of conformations only accessible in longer timescale under neutral pH (Fig. S3).

Consistent with the converging data on long timescale motions, multiple transitions between conformational substates are observed for residues with motions in the supra-τ_c range (Figs. 3, 4, 6, and Fig. S2). Such frequent transitions are essential to get accurate averages for the S^2_{LS} order parameters; in case the motional freedom of the N-H bond vector is significantly different in the populated substates. Indeed, we find that the decay of the correlation function of the N-H bond is different in the substates populated (Fig. 3). Sampling of one substate alone would, therefore, result in a too high or too low S^2_{LS} order parameter (see Table SI.3). The importance of sampling of substates accessible to a protein in the supra-τ_c timescale for the accurate

determination of S^2_{LS} order parameters has been underlined recently by Bouvignies et al. (43). They attributed an improved agreement between experimentally determined and simulation-based S^2_{LS} order parameters to efficient sampling by accelerated MD simulations (43).

The different substates sampled by residues with supra-τ_c motions are characterized by different backbone dihedral angles and significantly different $^3J_{HNH\alpha}$ coupling constants (Fig. 6 and Fig. S2). Residue L12 of the β-strand 2 that mediates interactions between protein Gβ1 and its antigen-binding partner IgG, for instance, shows a very broad bimodal distribution of its J-coupling constants (Fig. S2). In contrast, L5 in the protein core has a narrow distribution of its $^3J_{HNH\alpha}$ coupling constants (Fig. 6 A). Overall, residues with supra-τ_c motions and broad distributions of their J-coupling constants are observed in the highly flexible region of β-strand 2 and in the turn connecting the helix and β-strand 3. Individually, or in combination, the supra-τ_c motions of these residues can lead to significant structural changes (see Fig. 6). One may speculate that these motions and structural changes have been exploited by nature for functional purposes as residues in the highly flexible region of β-strand 2 mediate interactions between protein Gβ1 and its antigen-binding partner IgG (17) and the turn connecting the helix and β-strand 3 is involved in dimerization (34). In line with our findings for Gβ1, Lange et al. (9) have recently shown that the conformational substates sampled in the supra-τ_c regime are important for rapid and specific molecular recognition of binding partners by ubiquitin (44).

CONCLUSIONS

We have described the sub-τ_c and supra-τ_c motions that exist in protein Gβ1 by applying the model-free approach to the autocorrelation functions of backbone bond vectors calculated from the 175 ns MD trajectory. The amplitudes of the motions that we observed are highly correlated to those derived from a range of NMR measurements probing motions on different timescales. The results that we presented indicate that by analyzing the autocorrelation functions in combination with the ^3J couplings, it is possible to characterize the dynamic transitions in the supra-τ_c regime that may be relevant for protein functions.

SUPPORTING MATERIAL

Three figures and three tables are available at http://www.biophysj.org/biophysj/supplemental/S0006-3495(09)01377-0.

REFERENCES

1. Mittermaier, A., and L. E. Kay. 2006. New tools provide new insights in NMR studies of protein dynamics. *Science*. 312:224–228.

2. Boehr, D. D., H. J. Dyson, and P. E. Wright. 2006. An NMR perspective on enzyme dynamics. *Chem. Rev*. 106:3055–3079.

3. Palmer, 3rd, A. G. 2004. NMR characterization of the dynamics of biomacromolecules. *Chem. Rev*. 104:3623–3640.

4. Igumenova, T. I., K. K. Frederick, and A. J. Wand. 2006. Characterization of the fast dynamics of protein amino acid side chains using NMR relaxation in solution. *Chem. Rev*. 106:1672–1699.

5. Lipari, G., and A. Szabo. 1982. Model-free approach to the interpretation of nuclear magnetic-resonance relaxation in macromolecules. *J. Am. Chem. Soc*. 104:4546–4559.

6. Tjandra, N., and A. Bax. 1997. Direct measurement of distances and angles in biomolecules by NMR in a dilute liquid crystalline medium. *Science*. 278:1111–1114.

7. Meiler, J., J. J. Prompers, W. Peti, C. Griesinger, and R. Bruschweiler. 2001. Model-free approach to the dynamic interpretation of residual dipolar couplings in globular proteins. *J. Am. Chem. Soc*. 123:6098–6107.

8. Tolman, J. R., H. M. Al-Hashimi, L. E. Kay, and J. H. Prestegard. 2001. Structural and dynamic analysis of residual dipolar coupling data for proteins. *J. Am. Chem. Soc*. 123:1416–1424.

9. Lange, O. F., N. A. Lakomek, C. Fares, G. F. Schroder, K. F. Walter, et al. 2008. Recognition dynamics up to microseconds revealed from an RDC-derived ubiquitin ensemble in solution. *Science*. 320:1471–1475.

10. Maragakis, P., K. Lindorff-Larsen, M. P. Eastwood, R. O. Dror, J. L. Klepeis, et al. 2008. Microsecond molecular dynamics simulation shows effect of slow loop dynamics on backbone amide order parameters of proteins. *J. Phys. Chem. B*. 112:6155–6158.

11. Adcock, S. A., and J. A. McCammon. 2006. Molecular dynamics: survey of methods for simulating the activity of proteins. *Chem. Rev*. 106:1589–1615.

12. Trbovic, N., B. Kim, R. A. Friesner, and A. G. Palmer, 3rd. 2008. Structural analysis of protein dynamics by MD simulations and NMR spin-relaxation. *Proteins*. 71:684–694.

13. Showalter, S. A., and R. Bruschweiler. 2007. Quantitative molecular ensemble interpretation of NMR dipolar couplings without restraints. *J. Am. Chem. Soc*. 129:4158–4159.

14. Markwick, P. R., G. Bouvignies, and M. Blackledge. 2007. Exploring multiple timescale motions in protein GB3 using accelerated molecular dynamics and NMR spectroscopy. *J. Am. Chem. Soc*. 129:4724–4730.

15. Barchi, Jr., J. J., B. Grasberger, A. M. Gronenborn, and G. M. Clore. 1994. Investigation of the backbone dynamics of the IgG-binding domain of streptococcal protein G by heteronuclear two-dimensional ^{1}H–^{15}N nuclear magnetic resonance spectroscopy. *Protein Sci*. 3:15–21.

16. Achari, A., S. P. Hale, A. J. Howard, G. M. Clore, A. M. Gronenborn, et al. 1992. 1.67-A x-ray structure of the B2 immunoglobulin-binding domain of streptococcal protein G and comparison to the NMR structure of the B1 domain. *Biochemistry*. 31:10449–10457.

17. Bouvignies, G., P. Bernado, S. Meier, K. Cho, S. Grzesiek, et al. 2005. Identification of slow correlated motions in proteins using residual dipolar and hydrogen-bond scalar couplings. *Proc. Natl. Acad. Sci. USA*. 102:13885–13890.

18. Clore, G. M., and C. D. Schwieters. 2004. Amplitudes of protein backbone dynamics and correlated motions in a small alpha/beta protein: correspondence of dipolar coupling and heteronuclear relaxation measurements. *Biochemistry*. 43:10678–10691.

19. Gronenborn, A. M., D. R. Filpula, N. Z. Essig, A. Achari, M. Whitlow, et al. 1991. A novel, highly stable fold of the immunoglobulin binding domain of streptococcal protein G. *Science*. 253:657–661.

20. Vriend, G. 1990. WHAT IF: a molecular modeling and drug design program. *J. Mol. Graph*. 8:52–56.

21. Gilson, M. K., and B. Honig. 1988. Calculation of the total electrostatic energy of a macromolecular system: solvation energies, binding energies, and conformational analysis. *Proteins*. 4:7–18.

22. Ulmer, T. S., B. E. Ramirez, F. Delaglio, and A. Bax. 2003. Evaluation of backbone proton positions and dynamics in a small protein by liquid crystal NMR spectroscopy. *J. Am. Chem. Soc.* 125:9179–9191.

23. Jorgensen, W. L., J. Chandrasekhar, J. D. Madura, R. W. Impey, and M. L. Klein. 1983. Comparison of simple potential functions for simulations liquid water. *J. Chem. Phys.* 79:926–935.

24. Hornak, V., R. Abel, A. Okur, B. Strockbine, A. Roitberg, et al. 2006. Comparison of multiple Amber force fields and development of improved protein backbone parameters. *Proteins*. 65:712–725.

25. Hornak, V., A. Okur, R. C. Rizzo, and C. Simmerling. 2006. HIV-1 protease flaps spontaneously open and closed in molecular dynamics simulations. *Proc. Natl. Acad. Sci. USA*. 103:915–920.

26. Case, D. A., T. E. Cheatham, T. Darden, H. Gohlke, R. Luo, et al. 2005. The Amber biomolecular simulation programs. *J. Comput. Chem.* 26:1668–1688.

27. Andersen, H. C. 1980. Molecular dynamics simulations at constant pressure and-or temperature. *J. Chem. Phys.* 72:2384–2393.

28. Darden, T., D. York, and L. Pedersen. 1993. Particle Mesh Ewald—an N.Log(N) method for Ewald sums in large systems. *J. Chem. Phys.* 98:10089–10092.

29. Ryckaert, J. P. C., G. Ciccotti, and H. Berendsen. 1977. Numerical integration of cartesian equations of motion of a system with constraints: molecular dynamics of n-alkanes. *J. Comput. Phys.* 23:327–341.

30. Redfield, A. G. 1965. The theory of relaxation processes. *Adv. Magn. Reson.* 1:1–32.

31. Clore, G. M., P. C. Driscoll, P. T. Wingfield, and A. M. Gronenborn. 1990. Analysis of the backbone dynamics of interleukin-1 beta using two-dimensional inverse detected heteronuclear ^{15}N–^{1}H NMR spectroscopy. *Biochemistry*. 29:7387–7401.

32. Chen, J., C. L. Brooks, 3rd, and P. E. Wright. 2004. Model-free analysis of protein dynamics: assessment of accuracy and model selection protocols based on molecular dynamics simulation. *J. Biomol. NMR*. 29:243–257.

33. Showalter, S. A., and R. Bruschweiler. 2007. Validation of molecular dynamics simulations of biomolecules using NMR spin relaxation as benchmarks: application to the AMBER99SB force field. *J. Chem. Theory Comput.* 3:961–975.

34. Byeon, I. J., J. M. Louis, and A. M. Gronenborn. 2003. A protein contortionist: core mutations of GB1 that induce dimerization and domain swapping. *J. Mol. Biol.* 333:141–152.

35. Chandrasekhar, I., G. M. Clore, A. Szabo, A. M. Gronenborn, and B. R. Brooks. 1992. A 500 ps molecular dynamics simulation study of interleukin-1 beta in water. Correlation with nuclear magnetic resonance spectroscopy and crystallography. *J. Mol. Biol.* 226:239–250.

36. Karplus, M. 1959. Contact electron-spin coupling of nuclear magnetic moments. *J. Chem. Phys.* 30:11–15.

37. Vogeli, B., J. Ying, A. Grishaev, and A. Bax. 2007. Limits on variations in protein backbone dynamics from precise measurements of scalar couplings. *J. Am. Chem. Soc.* 129:9377–9385.

38. Bruschweiler, R., and D. A. Case. 1994. Adding harmonic motion to the Karplus relation for spin-spin coupling. *J. Am. Chem. Soc.* 116:11199–11200.

39. Hu, J. S., and A. Bax. 1998. Measurement of three-bond, ^{13}C′-^{13}C beta J couplings in human ubiquitin by a triple resonance, E. COSY-type NMR technique. *J. Biomol. NMR*. 11:199–203.

40. Lindorff-Larsen, K., R. B. Best, and M. Vendruscolo. 2005. Interpreting dynamically-averaged scalar couplings in proteins. *J. Biomol. NMR*. 32:273–280.

41. Clore, G. M. 1999. Structures of B1 domain of streptococcal protein G. *J. Am. Chem. Soc.* 121:2337–2338.

42. Gronenborn, A. M., and G. M. Clore. 1993. Identification of the contact surface of a streptococcal protein G domain complexed with a human Fc fragment. *J. Mol. Biol.* 233:331–335.

43. Bouvignies, G., P. Markwick, R. Bruschweiler, and M. Blackledge. 2006. Simultaneous determination of protein backbone structure and dynamics from residual dipolar couplings. *J. Am. Chem. Soc.* 128:15100–15101.

44. Penengo, L., M. Mapelli, A. G. Murachelli, S. Confalonieri, L. Magri, et al. 2006. Crystal structure of the ubiquitin binding domains of rabex-5 reveals two modes of interaction with ubiquitin. *Cell*. 124:1183–1195.